Radiographic Imaging

7

Nikolaos Kartalis and Johannes Matthias Löhr

Introduction

For the radiological investigation of the various pancreatic masses, there is a wide variety of available imaging modalities, such as computed tomography (CT), magnetic resonance imaging (MRI), ultrasonography (US), and nuclear medicine. In this chapter, a short overview of the available techniques with an emphasis on recent advances will be presented, followed by a practical diagnostic imaging algorithm. Finally, the imaging features of the most common solid and cystic pancreatic lesions will be illustrated.

Imaging Techniques

In order to obtain optimal results, it is necessary to apply dedicated imaging protocols depending on the relevant clinical scenario, where careful attention should be paid to technical parameters related to the scanner, the patient, and the intravenous contrast material potentially to be used.

Computed Tomography

CT is the "workhorse" in the imaging of pancreatic masses. In modern scanners, multiple, parallel positioned detector rows (MDCT) combined with a fast rotating X-ray tube enable imaging of the thorax and abdomen within a single breathhold. Thus, breathing-related motion artifacts can be minimized and an optimal use of iodine-based contrast material achieved, according to well-defined imaging protocols.

For the investigation of pancreatic masses, the upper abdomen (defined as the abdominal area between the diaphragm and the iliac crest) is scanned before (unenhanced) and after the intravenous injection of iodine-based contrast material in the late arterial (parenchymal or portal venous inflow) phase and the whole abdomen in the venous (or portal venous) phase (dynamic contrast-enhanced CT, DCE-CT) [1]. In order to account for intraindividual variations of heart rate between patients, the use of individualized delay between contrast agent injection and image acquisition is encouraged [2]. The image acquisition is performed in the axial plane and the resulting images (the so-called raw data) have a slice thickness in the range of millimeters or even submillimeters. These are then reconstructed in thicker

N. Kartalis (✉)
Division of Medical Imaging and Technology, Department of Clinical Science, Intervention and Technology (CLINTEC), Karolinska Institutet, and Department of Radiology, Karolinska University Hospital, C1-46, KS Huddinge, Stockholm 14186, Sweden
e-mail: nikolaos.kartalis@karolinska.se

J.M. Löhr
Division of Surgery, Department of Clinical Science, Intervention and Technology (CLINTEC), Karolinska Institutet, and Centre for Digestive Diseases, Karolinska University Hospital, Stockholm, Sweden

M.S. Wagh, P.V. Draganov (eds.), *Pancreatic Masses*, DOI 10.1007/978-3-319-19677-0_7

slices, preferably ≤3 mm, two-dimensional (2D) images in the axial, coronal, and sagittal planes (multi-planar reformats, MPRs) [1]. Occasionally, curved planar reformats (CPR) along the ductal system and/or major vasculature may also be of value [3]. If needed, e.g., for the depiction of the vascular anatomy, 2D maximum intensity projection (MIP) and three-dimensional (3D) volume-rendering technique (VRT) images can easily be reconstructed from the same data and provide additional information about vessel engagement [4–7]. Recent advances in the commercially available hard- and software have made possible the more precise quantification of abdominal organ and tissue perfusion characteristics by applying CT perfusion technique. Parameters like blood flow, blood volume, mean transit time, and the permeability–surface area product can be calculated, providing potentially valuable information about the hemodynamic characteristics of organs, tissues, and tumors [8].

Magnetic Resonance Imaging

MRI is particularly useful in the investigation of pancreatic masses. Due to its superior soft tissue contrast resolution [i.e., the ability to distinguish different structures from each other based on their signal intensity (SI) differences on the various imaging sequences] compared to CT and to the fact that it does not expose the examined area to potentially harmful ionizing radiation, it has become a modality of great interest. Drawbacks related to its use are the limited availability and the timely image acquisition, compared to CT, as well as the considerable variation in image quality between various MRI scanners. The magnetic field strength in modern equipment is either 1.5 or 3 T and dynamic contrast imaging is feasible within reasonable timeframes (i.e., a single breath-hold).

Similarly to the DCE-CT, MR image sequences are obtained before and after the intravenous administration of gadolinium-based chelates in late arterial, portal venous, and, additionally, equilibrium phases (dynamic contrast-enhanced MRI, DCE-MRI) [9]. The sequences used for the dynamic contrast imaging are fat-saturated 3D T1-weighted and can be primarily obtained in any plane, preferably the axial, with a slice thickness of 2–3 mm. The possibility to obtain MPRs from the originally acquired axial images exists, but the results may be of lower quality compared with CT examinations due to the lower spatial resolution, at least on 1.5 T scanners. Apart from these, the protocol should include magnetic resonance cholangiopancreatography (MRCP) and T2-weighted sequences, in order to depict the relation of the lesion(s) to the main pancreatic (MPD) and common bile (CBD) ducts and to demonstrate the internal architecture of the lesions without needing to use intravenous contrast material. Diffusion-weighted imaging (DWI) is a relatively new sequence implemented in abdominal applications. It is based on the random translational movement of free water molecules (or Brownian motion), which is restricted in cases where the extracellular space is diminished (such as when there is tumor-related hypercellularity and/or increased fibrosis) [10]. By calculating the apparent diffusion coefficient (ADC), it is possible to obtain objective measurements of the diffusivity in a given tissue or organ. For this calculation, various models are available. Among them are the automated monoexponential model, which is easier and faster, and the biexponential (intravoxel incoherent motion, IVIM) model, which is more complex and accurate and allows for, besides ADC calculations, the extraction of the following parameters: the slow component of diffusion (D_{slow}), incoherent microcirculation, or otherwise pseudodiffusion, (D_{fast}), and perfusion fraction (f) [11]. Similarly to CT, the MRI perfusion technique has recently been made available in advanced scanners and the acquisition of quantitative information about perfusion characteristics is now possible [12]. Parameters that can be extracted from MRI perfusion data are the following: the volume transfer coefficient (K^{trans}), the volume of extracellular extravascular space (EES), the per-unit volume of tissue (v_e), and the flux rate constant between EES and plasma (k_{ep}) [13]. However, MRI perfusion is a technically more demanding method compared to its CT counterpart [14].

Ultrasonography

US can also be used in the investigation of pancreatic tumors. There are various approaches to perform pancreatic US, such as transabdominally (i.e., examination through the abdominal wall), endoscopically (by inserting the transducer via an endoscope, EUS), and intraoperatively (by direct contact with the organ surface during operation, IOUS). This modality is advantageous in that it does not expose the area under investigation to ionizing radiation and allows a dynamic examination of the organ of interest by injecting microbubble-containing contrast agents [15, 16]. Finally, US is useful in providing biopsy guidance (for both fine-needle aspiration and core biopsy). The use of low-frequency transducers is suggested for examining deeper areas, where higher penetration is required, and of high-frequency transducers for more superficial areas. Drawbacks include the high operator dependency, the fact that secondary readings and optimal communication of findings to clinicians are somehow difficult to perform, the insufficient visualization in cases of obese patients or due to obscuring overlying intestinal gas (in case of the transabdominal approach), and, finally, the limited availability (in the case of EUS).

Nuclear Medicine

Nuclear medicine imaging may be useful in the workup of pancreatic masses, particularly for the investigation of pancreatic neuroendocrine tumors (PNETs). In general, the technique is based on the use of radioactive tracers and can be, grossly, divided into two subcategories: (1) scintigraphy and (2) positron emission tomography (PET). The combination of these with a cross-sectional modality (i.e., CT and lately even MRI) results in the so-called hybrid imaging.

Scintigraphy

In scintigraphy, a gamma (γ) camera detects γ rays emitted from the radionuclides used. The resulting images are either 2D whole-body (planar imaging) or 3D SPECT (single photon emission computed tomography) axial images of the abdominal area. In planar imaging, the acquisition is at 4 and 24 h after injection of the radioisotope while in SPECT at 24 h.

For the workup of PNETs, the vast majority of radiotracers used are somatostatin analogs (SSA) based on the expression of somatostatin receptors (SSR) in the majority of PNETs [17]. Octreotide is the most commonly used analog for somatostatin receptor scintigraphy (SRS) and is commercially widely available as ^{111}In-pentetreotide (^{111}In-DTPA-octreotide, Octreoscan™). Apart from the SSA, other analogs for imaging a subclass of PNETs based on their expression of the glucagon-like peptide 1 (GLP-1) receptor (i.e., benign insulinomas) have been developed. Their use is limited for research purposes and they are not yet clinically available.

Positron Emission Tomography

In PET, the radionuclides used emit positrons. When an emitted positron encounters an electron, they annihilate and emit two photons in opposite directions and are, consequently, detected by the PET camera at the same moment. Compared to scintigraphy, image acquisition can be completed within much shorter time intervals, resulting in images of higher spatial resolution and tissue contrast. Drawbacks include the short half-life of the radionuclides and the relatively complicated process of the labeling procedure. Two major types of radiotracers are used: those reflecting tumor activity and those related to receptor expression [18].

The first category comprises amine precursors such as ^{11}C-5-hydroxytryptophan (^{11}C-5-HTP), ^{18}F-DOPA, and ^{11}C-L-DOPA as well as the glucose analog ^{18}F-fluorodeoxyglucose (FDG). ^{18}F-FDG is by far the most widely available and well-studied radiotracer in PET imaging, while amine precursors are less widely available but can be valuable in cases where the suspected tumors are expected to have low SSR expression (in cases of PNET). For the production of all these radiotracers, a cyclotron is required.

The second category includes all available SSAs labeled with a positron emitter, mainly ^{68}Ga, and is therefore suited only for the imaging

evaluation of PNETs. In practice, the most often used preparations are ^{68}Ga-DOTATOC, ^{68}Ga-DOTANOC, and ^{68}Ga-DOTATATE (collectively termed ^{68}Ga-DOTA-SSA). These three exhibit some differences in the affinity to the SSR-subtypes 2, 3, and 5, which, however, are not significant for clinical practice. The production of ^{68}Ga does not need a cyclotron but can easily be generated in standard equipment available at nuclear medicine departments. Image acquisition can be done within an hour from injection of the radiotracer. Compared to the SSAs used in scintigraphy, ^{68}Ga-SSAs for PET imaging still have less availability.

Hybrid Imaging

In modernscanners, nuclear medicine modalities such as PET and SPECT are combined with a cross-sectional counterpart such as CT or, lately, even MRI [18, 19]. In that way, anatomical and functional images can be viewed simultaneously and findings in one modality can be directly correlated to the other. Furthermore, "fusion" images, where one image set is overlaid to the other, are available for easier evaluation. The cross-sectional examination can be performed according to dedicated contrast-enhanced protocols, as mentioned earlier in the corresponding section, for not compromising the diagnostic quality. Furthermore, data from CT are available for attenuation correction of the PET images, making the procedure more time-efficient compared to PET.

Diagnostic Imaging Algorithm

In case there is suspicion of a pancreatic cancer or the presence of a dilated MPD or/and CBD (in the latter case, the so called "double-duct" sign), a dedicated pancreatic protocol CT or MRI is indicated, as these are considered equivalent in determining engagement of vessel and lymph nodes, according to the recommendations by NCCN [1]. On the one hand, if a mass is then detected on CT (at most institutions, CT is the first-line modality) and there are no signs of metastatic disease, CT of the thorax and liver function tests should be performed and the patient discussed at a multidisciplinary tumor board as a potential surgical candidate. EUS should also be considered. On the other hand, if a mass is not detected, then besides CT of the thorax and liver function tests, EUS or ERCP or MRI/MRCP are indicated [1]. If the initial CT examination of the patient is high-quality, no further examination is considered necessary. For the detection of small liver and peritoneal metastases, it has been shown that MRI is superior to CT [20, 21]; thus, it may be considered a complement to CT in patients with a high risk for liver metastases when the initial examination failed to demonstrate them. The role of PET/CT is yet not clear; it was not shown beneficial for detecting early cancer but may prove useful for identifying extrapancreatic distant disease in "high-risk" patients [1].

In case there is suspicion of PNETs, the European Neuroendocrine Tumor Society's (ENETS) suggested workup algorithm includes pancreatic protocol CT or MRI and an additional SRS (or ^{68}Ga-DOTA-SSA PET/CT, when available) for the selection of patients eligible for treatment with radiolabeled SSA (peptide receptor radionuclide therapy; PRRT) [17]. When major surgery is an option and CT/MRI or SRS does not confirm the presence of tumor, then the next steps are ^{68}Ga-DOTA-SSA PET/CT and/or ^{18}F-DOPA and ^{11}C-5-HTP (if available); ^{18}F-FDG PET/CT may also be considered. In all PNET cases where the proliferation index Ki-67 is greater than 10 %, ^{18}F-FDG PET/CT should be considered.

When a cystic lesion is detected and further characterization is required, dedicated pancreatic protocol CT and MRI are considered particularly valuable [22]. For incidentally detected cystic lesions, MRI is the method of choice proposed by the Incidental Findings Committee of the American College of Radiology due to its superior contrast resolution [23]. ^{18}F-FDG PET/CT is potentially advantageous for detecting distant disease in cases of invasive carcinoma, but its role for the characterization of cystic masses is unclear, as data are not sufficient [22]. For their

cross-sectional imaging follow-up, the currently most widely established management guidelines favor the use of contrast-enhanced MRI [24, 25]. However, some preliminary reports have shown that—for the purpose of follow-up—unenhanced MRI may be adequate [26, 27].

Imaging Features

The imaging features of the most common solid and cystic masses of the pancreas as well as their differential diagnosis will be presented in the following section. Further details of each of these lesions are discussed separately in other chapters in this book.

Solid Masses

Pancreatic ductal adenocarcinoma (PDAC) and neuroendocrine tumors (PNETs) comprise together about 90–95 % of all malignant pancreatic neoplasms [28, 29].

Adenocarcinoma: PDAC, being a predominantly hypovascular fibrotic tumor, is usually depicted as a mass of lower density (on CT) or lower SI (on MRI) compared to the adjacent, avidly enhancing parenchyma during the late arterial phase of the dynamic contrast imaging (Figs. 7.1, 7.2a–d and 7.3) [30, 31]. Additional imaging features on MRI include hypointensity on unenhanced T1-weighted and variable appearance on

Fig. 7.1 Dedicated pancreatic protocol CT examination of a patient with a pancreatic ductal adenocarcinoma. In the dynamic contrast-enhanced (DCE) axial images [unenhanced (**a**), late arterial (**b**), and portal venous (**c**) phases], there are an ill-defined, hypovascular mass at the pancreatic body (*arrow*) with upstream parenchymal atrophy (*arrowhead*) and a hypovascular solid lesion in the left hepatic lobe (*asterisk*), compatible with a metastasis. In the sagittal MIP image (**d**) and coronal projection (**e**) (both at the late arterial phase), there are tumor encasement and stricturing of all branches of the celiac trunk (*open arrows*). In the axial MIP image of the portal venous phase (**f**), the stenosis of portomesenteric confluence (*open arrowhead*) is readily identified

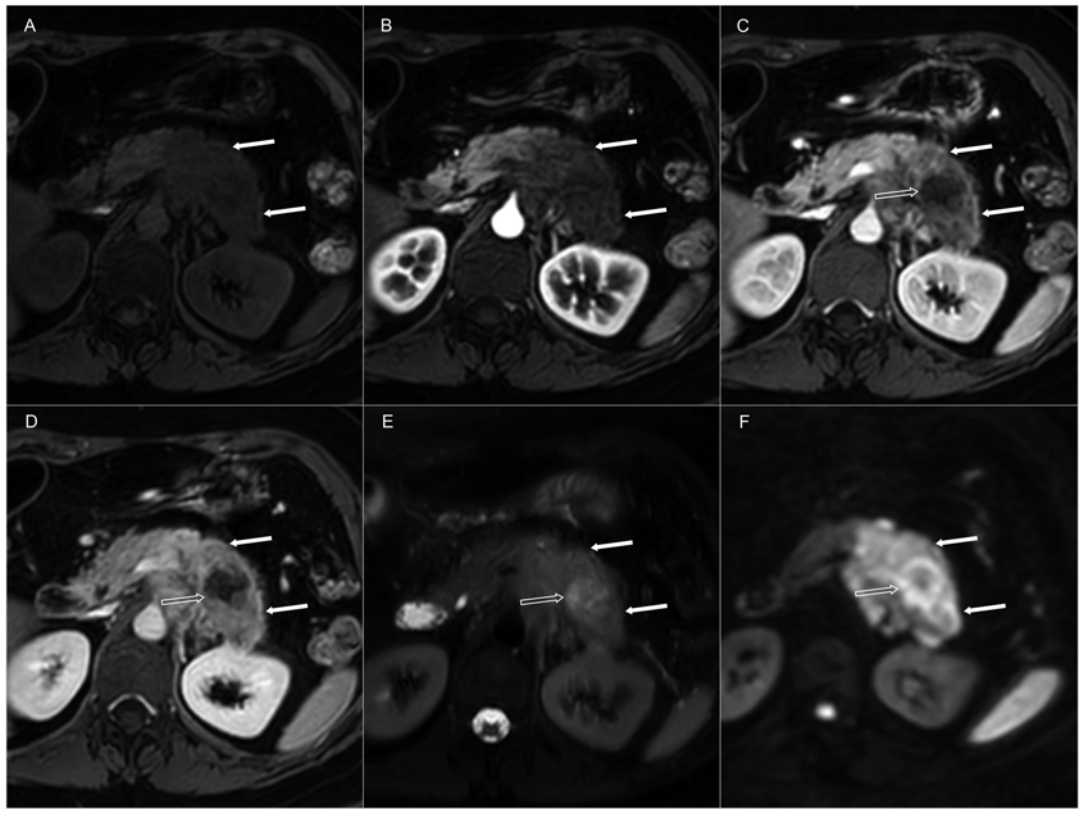

Fig. 7.2 Dedicated pancreatic protocol MRI examination of a patient with a pancreatic ductal adenocarcinoma. In the unenhanced image (**a**), the mass located at the proximal tail (arrows) has a lower signal intensity (SI) compared to the downstream normal parenchyma. The mass is hypovascular compared to the avidly enhancing parenchyma in the late arterial phase (**b**) of the DCE series and shows progressive enhancement in the portal venous (**c**) and equilibrium (**d**) phases, where even a central necrotic area (*open arrow*) is observed. Compared to the normal parenchyma, the mass has a slightly higher SI on the T2-weighted image (**e**) and a much higher SI on DWI with a high *b*-value (**f**), indicating restricted diffusion

T2-weighted sequences. On visual assessment of DWI, the lesion usually exhibits high SI on images with high *b*-values and low SI on ADC maps representing restricted diffusion (Fig. 7.2). The margins of the lesion are often not well defined and, in many cases, there are secondary signs indicating the presence of a tumor, such as main pancreatic or/and common bile duct dilation and/or abrupt cutoff, upstream obstructive pancreatitis with parenchymal atrophy or focally abnormal parenchymal contour. In about 5 % of cases, the tumor may not be distinguished from the adjacent parenchyma on CT, even when dedicated protocols are applied (Fig. 7.4) [32, 33]. In such cases, the presence of secondary tumor signs combined with a further evaluation with other methods (EUS/MRI/PET-CT) may prove helpful. For the evaluation of engagement of vessels and lymph nodes, dedicated pancreatic CT and MRI are considered equivalent [1]. However, size as a criterion of lymph node engagement has been shown not to be specific [34].

In the differential diagnosis, PDAC has to be distinguished from other solid hypovascular lesions (Table 7.1) [35]. A major diagnostic challenge is to correctly differentiate adenocarcinoma from an inflammatory pseudotumor, such as in cases of mass-forming chronic pancreatitis (CP), focal autoimmune pancreatitis (AIP), and groove pancreatitis (Fig. 7.5). In cases of mass-forming CP, MRCP is of great value when it depicts the pancreatic duct passing through the suspicious

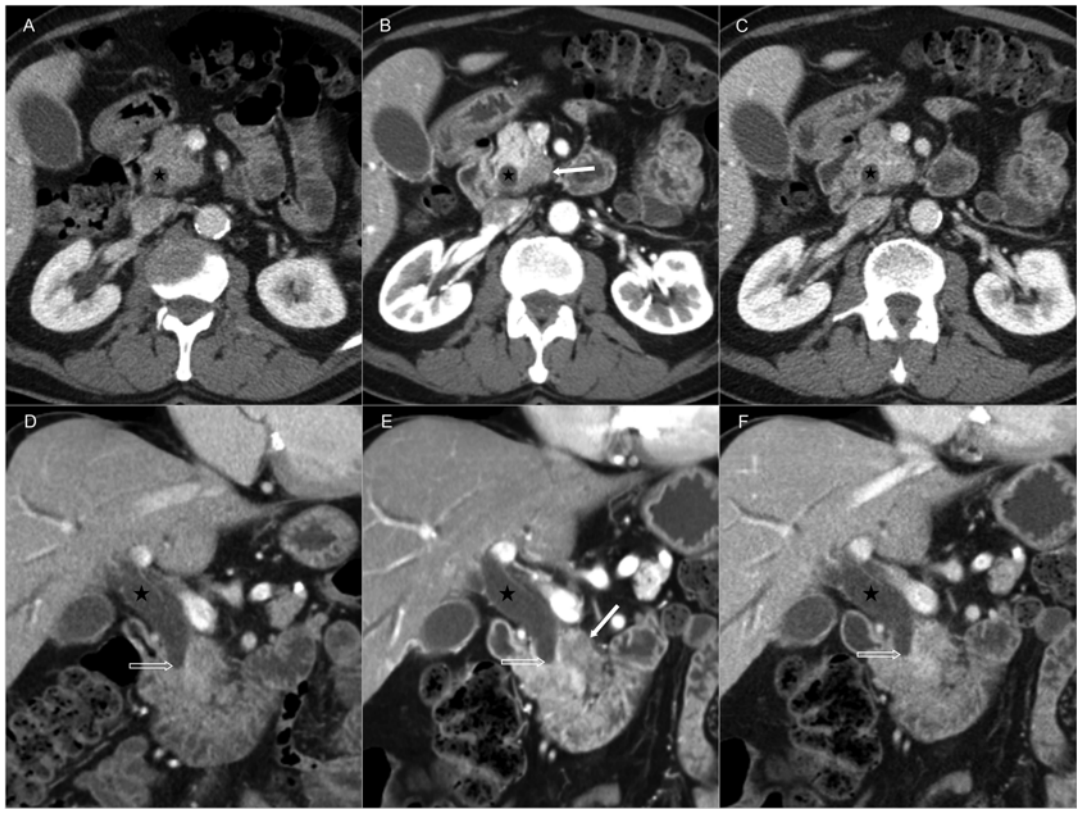

Fig. 7.3 Axial (**a**–**c**) and coronal (**d**–**f**) CT images of a patient presenting with mild pain in the upper abdomen, fatigue, and itching. The nondedicated contrast-enhanced CT protocol (**a**, **d**) performed at the emergency setting shows dilation of the common bile duct (*asterisk*) with abrupt cutoff at the level of the pancreatic head (*open arrow*) but fails to demonstrate any mass. Two days later, the patient undergoes a dedicated pancreatic protocol CT and the hypovascular mass (*arrow*) is readily identified at the pancreatic head/uncinate process in the late arterial (**b**, **e**) but not in the portal venous phase (**c**, **f**) of the DCE imaging. The lesion was a ductal adenocarcinoma, verified histopathologically after surgery (pancreatico-duodenectomy)

area, the so-called duct-penetrating sign, favoring nonmalignancy [36]. In cases of AIP, there might be a long compression of the MPD without a prominent upstream dilatation, a sausage-like appearance of the gland, and an enhancing soft-tissue halo in the peripancreatic fat as well as signs of extrapancreatic manifestation of autoimmune disease, such as in the bile duct, gallbladder, retroperitoneum, and more [37]. After appropriate cortisone therapy, there should be a partial or complete response of the radiological findings. Recently developed techniques such as CT perfusion, MRI perfusion, and DWI have shown promising results [38–41]. Particularly for DWI, the IVIM-derived parameter perfusion fraction (*f*) was shown to be significantly lower in cases of PDAC compared to CP and thus helpful for their differentiation [42, 43]. Furthermore, ^{18}F-FDG PET/CT has been reported to be able to differentiate mass-forming pancreatitis from adenocarcinoma by showing standardized uptake value (SUV) between 3 and 4 for chronic pancreatitis and >4 for PADC [44] and AIP from PDAC by demonstrating different patterns of radiotracer uptake (more commonly diffuse uptake in the pancreatic parenchyma and salivary glands observed in cases of AIP, while in cases of PDAC, there is focal accumulation in the tumor but not in the rest of the parenchyma) [45, 46].

Neuroendocrine tumors: Contrary to adenocarcinomas, PNETs are often highly vascularized

Fig. 7.4 Axial (**a**, **b**) and coronal (**c**, **d**) images of a dedicated pancreatic protocol CT of a patient presenting with fever, leukocytosis, elevated CRP, and liver function tests one month after endoscopic removal of CBD stent. The nondedicated CT protocol (not shown) performed two days earlier was not conclusive. No tumor can be visualized in the late arterial (**a**, **c**) or portal venous (**b**, **d**) phase of the DCE imaging despite the application of the dedicated protocol. However, secondary signs such as dilated main pancreatic duct in the upper part of the pancreatic head with abrupt cutoff in the upper part of the pancreatic head (*arrow*) may indicate the presence of a tumor. At histopathology after surgery, the presence of a small ductal adenocarcinoma was verified

Table 7.1 Differential diagnosis of pancreatic ductal adenocarcinoma (PDAC)

Inflammatory pseudotumors
Mass-forming chronic pancreatitis
Focal autoimmune pancreatitis
Groove pancreatitis
Nonhypervascular neuroendocrine tumors
Hypovascular metastases (e.g., lung cancer)
Lymphoma

Source: From [35]

tumors, which lead to the classical appearance of a hyperdense (on CT) or hyperintense (on MRI) mass during the late arterial phase of the dynamic contrast imaging (Fig. 7.6a–c) [47]. Nevertheless, there are exceptions with some PNETs—more often nonfunctioning—not showing hypervascularity but a rather heterogeneous contrast enhancement (Fig. 7.7) [47]. Calcifications are present in every sixth to eighth patient and are readily identified on unenhanced CT (Fig. 7.6a) [48, 49]. Additional typical imaging features on MRI include low SI on T1-weighted and high SI on T2-weighted sequences and restricted diffusion on DWI (Fig. 7.7a,e,f). Unlike adenocarcinomas, PNETs are usually well circumscribed and dilation of the MPD and/or CBD is less commonly present [50]; duct dilation, however, may be present, more often in cases of small serotonin-producing tumors [51]. Recently, it was reported that for the detection of highly differentiated PNETs, the visual assessment of DWI had the same detection rate as the

Fig. 7.5 Axial (**a**–**c**) and coronal (**d**–**f**) images of three different patients with solid hypovascular lesions (*arrows*) at the pancreatic head with secondary mild to moderate dilation of the main pancreatic duct and abrupt cutoff, simulating pancreatic ductal adenocarcinoma. The histopathological analysis after surgery showed mass-forming chronic pancreatitis in the first patient (**a**, **d**) and focal autoimmune pancreatitis in the second (**b**, **e**). In the third patient (**c**, **f**), changes of groove pancreatitis are identified radiologically (at 3-year control CT examination, no signs of malignancy had developed in the area)

contrast-enhanced MRI, in a lesion- and patient-based analysis [52]. This may prove to be of great value in cases where the intravenous injection of MRI contrast agents is contraindicated (e.g., in patients with low GFR or previous allergic reactions to gadolinium chelates).

At Octreoscan and ^{68}Ga-DOTA-SSA PET/PET-CT, PNETs exhibit, in general, high radiotracer uptake (Fig. 7.6d, e). ^{68}Ga-DOTA-SSA imaging performs better than Octreoscan [17]; however, both have lower detections rates for insulinomas compared to other PNETs [53]. Interestingly, for benign insulinomas, scintigraphy with GLP-1 analogs has shown promising initial results [54].

For the staging of PNETs, both the CT perfusion-extracted parameter blood flow and the monoexponential-based ADC calculations were shown to be significantly higher for G1 compared to G2 and G3 tumors [55–57]. In the latter report, G1 tumors were also significantly more often hypervascular, showing contrast enhancement after the intravenous injection of gadoxetic acid, compared to G2 and G3 tumors. Furthermore, the MRI perfusion-extracted parameter K^{trans} was reported to be significantly higher in G1 and G2 and could, thus, differentiate them from G3 PNETs [39]. In the differential diagnosis, PNETs have to be distinguished from other hypervascular lesions (Table 7.2) [58].

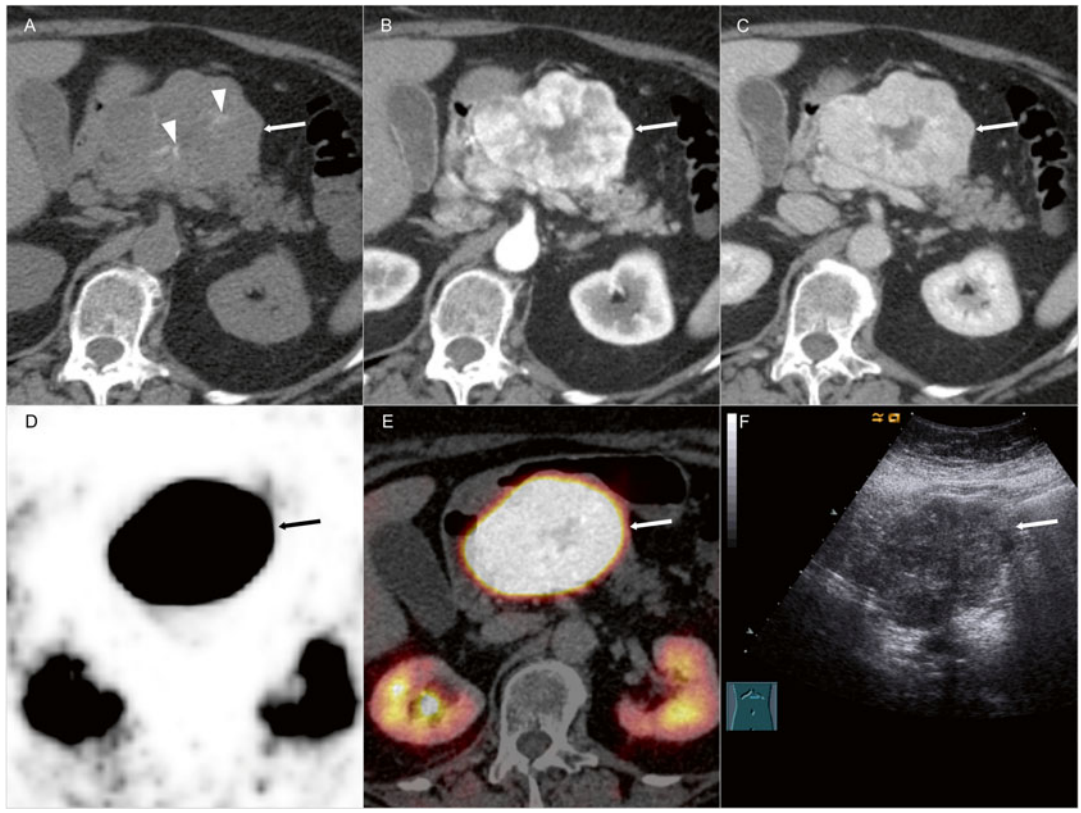

Fig. 7.6 Typical imaging findings of a patient with a neuroendocrine tumor in the pancreatic body. In the axial unenhanced CT image (**a**), the lobulated, well-defined mass (*arrow*) has central calcifications (*arrowheads*) and in the DCE imaging [late arterial (**b**) and portal venous (**c**) phase] it exhibits rapid, relatively inhomogeneous contrast enhancement. There is no upstream dilation of the main pancreatic duct. In the axial 68Ga-DOTATOC PET (**d**) and fusion 68Ga-DOTATOC PET/CT image (**e**), the lesion has very strong radiotracer uptake while at transabdominal ultrasound (**f**), it is relatively inhomogeneous and with low echogeneity

Cystic Masses

Serous cystic adenomas (SCAs), mucinous cystic neoplasms (MCNs), and intraductal papillary mucinous neoplasms (IPMNs) comprise about 90 % of all primary cystic lesions [59].

Serous Cystic Adenoma: The radiological appearance of an SCA depends on the histopathological type; it is usually classified in the microcystic (also known as polycystic) and the, much less frequent, macrocystic (also known as oligocystic) variants [60–62].

Microcystic SCAs, due to the presence of multiple, fluid-filled cysts <2 cm, separated from each other by thin septae, with the smaller cysts located centrally around fibrous tissue (central scar) and the larger ones in the periphery, have a multilobular shape with well-defined margins. The fibrous central scar can be partially calcified in up to one third of patients [63]. In about 20 % of cases, the comprising cysts are very small and the lesion can resemble a solid tumor (honeycomb pattern) [61]. More specifically on US, the cystic parts are hypoechoic while the septa and central scar are hyperechoic; in case of a honeycomb pattern, the tumor may appear entirely solid, that is, homogeneously hypoechoic with no posterior acoustic enhancement. The calcifications are depicted as centrally located

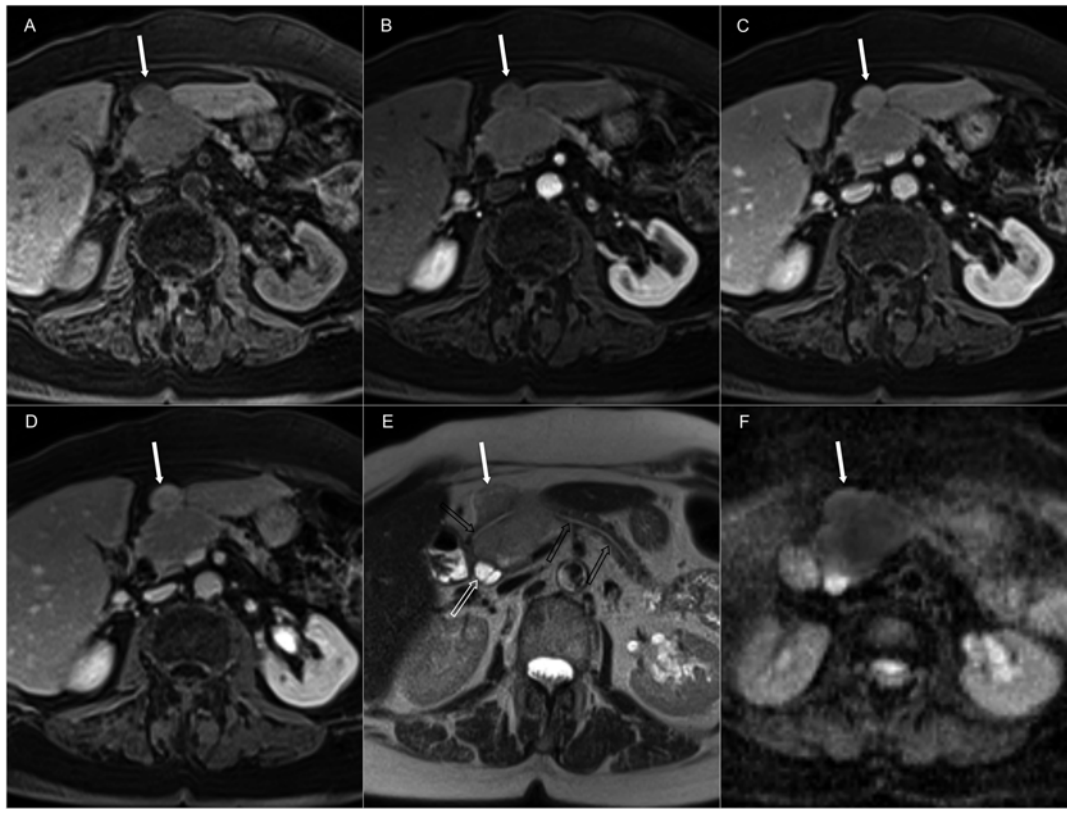

Fig. 7.7 MRI examination of a patient with a nonhypervascular neuroendocrine tumor in the proximal body of the pancreas. On fat-saturated T1-weighted images before (**a**) and post contrast (**b–d**), the tumor (*white arrow*) does not show hypervascularity, a finding more common in nonfunctioning PNETs. On the T2-weighted HASTE image (**e**), the tumor shows relatively high signal intensity and its relation to the common bile duct (*open white arrow*) and the main pancreatic duct (*open black arrows*) can easily be appreciated. On the ADC map (**f**), the lesion has markedly low signal intensity, indicating restricted diffusion

Table 7.2 Differential diagnosis of pancreatic neuroendocrine tumors (PNETs)

Exocrine tumors
Cystic: Serous cystic adenoma
Solid: Solid pseudopapillary neoplasia, acinar cell carcinoma
Hypervascular metastases
Renal cell carcinoma
Carcinoid
Medullary thyroid carcinoma
Multiple myeloma
Neurogenic
Schwannoma
Vascular
Aneurysm
Pseudoaneurysm
Arteriovenous malformation, AVM
Developmental
Intrapancreatic splenule (accessory spleen)

Source: Modified from Bhosale et al. [58]

hyperechoic structures with acoustic shadowing. On unenhanced CT, the lesion has low density and the calcifications are readily identified as central hyperdensities. On postcontrast CT, there is relatively rapid enhancement of the septa while the cystic portions remain hypodense due to the presence of nonenhancing fluid (Fig. 7.8a–c). In cases of lesions exhibiting a honeycomb pattern, the enhancement can be fairly homogeneous and, thus, closely resemble a solid tumor [64]. On T2-weighted images, the cystic portions of the lesions have a distinctly high SI while the septae

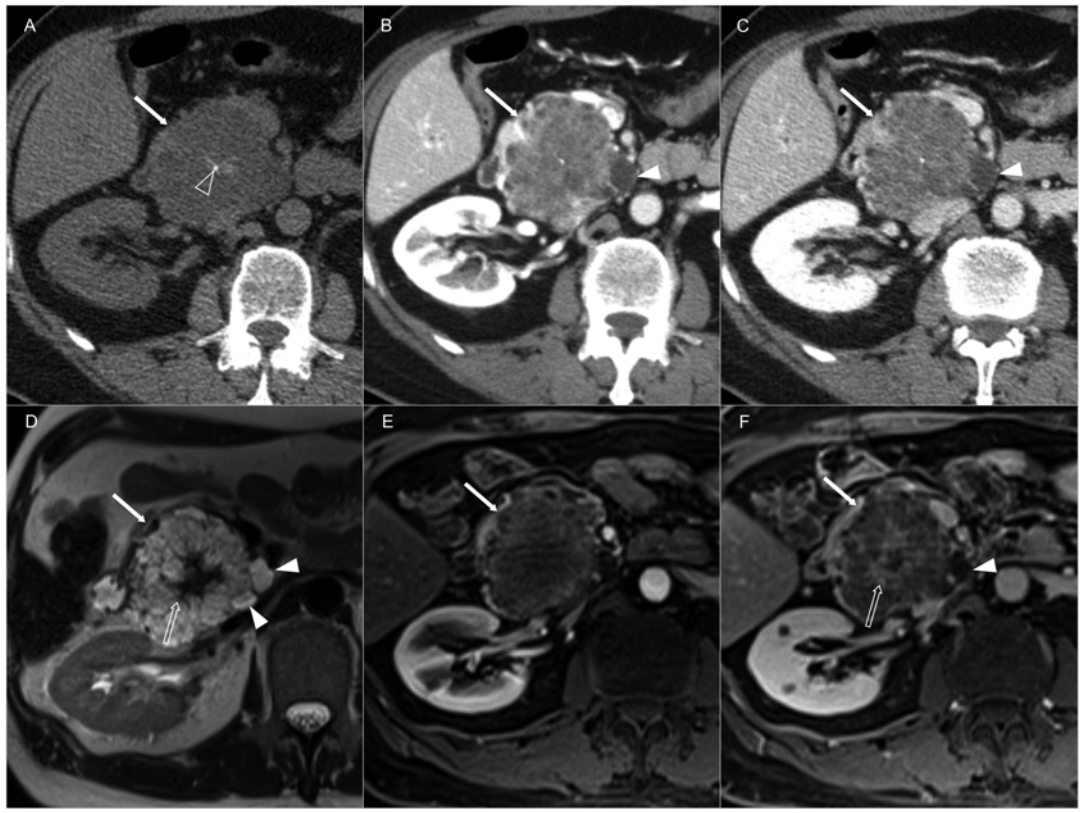

Fig. 7.8 Typical imaging findings of a patient with microcystic serous cystic adenoma. In the axial unenhanced CT image (**a**), the lesion (*arrow*) has central calcifications (*open arrowhead*) and in the DCE imaging [late arterial (**b**) and portal venous (**c**) phases], it shows relatively early, mild contrast enhancement. It is composed of multiple very small cysts in the central part and a few larger cysts in the periphery (*arrowheads*); the internal structure is much easier to appreciate in the axial T2-weighted MRI image (**d**). The central scar (*open arrow*) has a low signal intensity and in the fat-saturated T1-weighted images shows no enhancement in the later arterial phase (**e**); however, there is obvious, late enhancement in the equilibrium phase (**f**)

and fibrous scar have a low SI (Fig. 7.8d). T2-weigthed images depict fluid content, even in cases of a honeycomb pattern, due to the superb contrast resolution of T2-weighted MRI compared to CT. On unenhanced T1-weighted MRI, both the cystic and the noncystic parts have a low SI, and in cases of intralesional hemorrhage, there might be hyperintense areas. On postcontrast images, there is enhancement of the septa, in an analogous manner to postcontrast CT, and additionally, in the later phases of the dynamic imaging, the central scar may retain contrast (Fig. 7.8e, f). Compared to CT, calcifications are more difficult to detect on T1- and T2-weighted images; if present, they are depicted as areas of signal void. The lesion does not show restricted diffusion [65]. The differentiation of microcystic serous adenoma includes other solid enhancing lesions, such as PNETs and solid pseudopapillary neoplasia (SPNs) [58].

The macrocystic SCA, due to the presence of only a few number of cysts that are usually >1 cm or, sometimes, even up to several cm in size, is also multilobulated and well circumscribed [61, 66]. They do not have a central scar, calcifications, or mural nodules. On US and CT, the

Fig. 7.9 Typical imaging findings of a patient with an oligocystic serous cystic adenoma. In the axial unenhanced CT image (**a**), the lesion in the pancreatic neck (*arrow*) has no calcifications. In the axial DCE imaging [late arterial (**b**) and portal venous (**c**) phases], there are few, very thin internal septations (*arrowhead*), which are more easily appreciated on T2-weighted sequences [axial (**d**) and coronal (**e**) T2-weighted images]. The lesion is comprised of a few cysts, larger in size compared to microcystic SCAs (Fig. 7.8) and there is no upstream dilation of the main pancreatic duct. In the postcontrast fat-saturated T1-weighted image (**f**), there are no signs of cyst wall thickening, nodularity, or abnormal enhancement

lesions have a fairly homogeneous cystic appearance with low echogeneity (respectively, density) and high SI on T2- and low SI on unenhanced T1-weighted MRI (Fig. 7.9). The few septa may be recognizable on US or postcontrast CT but are more readily visible on T2- and postcontrast T1-weighted images, due to the superb contrast resolution (Fig. 7.9d–f). In contrast to their microcystic counterparts, macrocystic SCAs may resemble MCNs or side-branch IPMNs, and their differentiation based on imaging features is not always possible, sometimes necessitating further workup (Fig. 7.10) [67, 68]. Furthermore, they need to be differentiated from pseudocysts and SPNs [61].

None of the two types of SCAs show communication with the MPD.

Mucinous Cystic Neoplasm: MCNs comprise a group of mucin-producing, cystic lesions with a varying grade of malignant potential, that is, from completely benign to invasive carcinoma [69–72]. The lesions are located in 75 % of cases in the body and tail of the pancreas [73]. They are

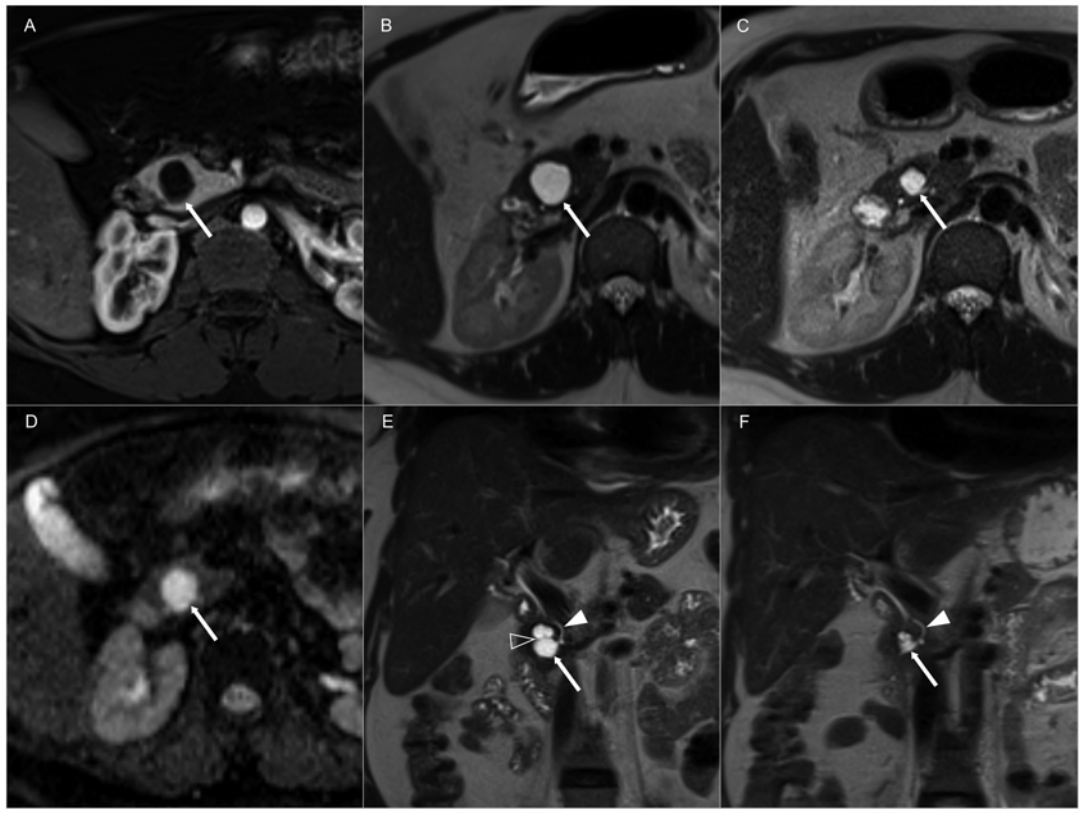

Fig. 7.10 MRI images of a patient with a cystic lesion at the pancreatic head at two different occasions. The lesion (*arrow*) shows no contrast enhancement (**a**), unrestricted diffusion on the ADC map (**d**), and one very thin internal septation (*open arrowhead*), easily identified on T2-weighted sequences [axial (**b**) and coronal (**e**) T2-weighted images]. The normal main pancreatic duct (*arrowhead*) is very close to the lesion, giving the impression of communicating with the cystic lesion. The lesion size increased from 1.2 (**c**, **f**) to 2.5 cm (**b**, **e**) during an interval of 18 months and, as there was suspicion of communication with the main pancreatic duct, it was considered a rapidly growing side-brunch IPMN. At histopathology after surgery, the lesion was shown to be an oligocystic serous cystic adenoma

encapsulated, well circumscribed, usually unilocular or, less commonly, multilocular (20 %) [60]. The presence of a thick capsule, internal septa, and solid components as well as peripheral or septal calcifications increases the risk of underlying malignancy [69, 74]. Relatively rarely, there might be intralesional hemorrhage. The lesion does not communicate with the MPD.

On US, the lesion has low echogeneity with posterior acoustic enhancement and can be homogeneous or heterogeneous, depending on the nature of its contents. A thickened capsule, the presence of septa, solid components, and, rarely, hemorrhagic products can be visualized as echogenic structures. Accordingly, calcifications can also be detected as echogenic structures with posterior acoustic shadow. On unenhanced CT, the lesion is usually hypodense and the internal architecture is not easy to delineate in detail. Calcifications in the periphery and/or in the central parts are readily identified (Fig. 7.11) [75]. On MRI, the internal architecture is easier to

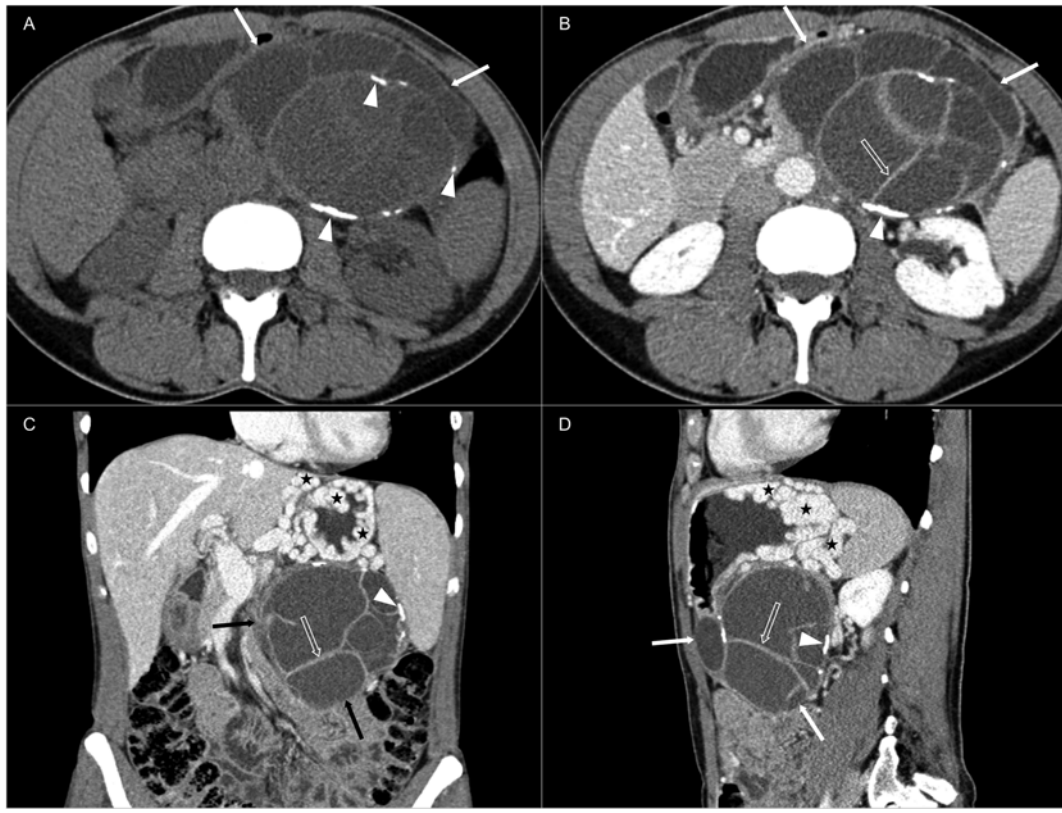

Fig. 7.11 Imaging features of a female patient with a large mucinous cystic neoplasm at the pancreatic body and tail on unenhanced (**a**) and contrast-enhanced (**b**–**d**) CT. The lesion (*arrows*) is multilocular, has peripheral and septal calcifications (*arrowheads*), and has relatively thick, contrast-enhancing internal septations (*open arrow*). Due to compression of the splenic vein, an extended network of varices (*asterisks*) has developed in the stomach and abdomen's left upper quadrant. On histopathology after surgery, there was up to high-grade dysplasia but no signs of invasive carcinoma

depict. On T2-weighted images, the lesion has markedly high SI, while the capsule, septations, mural nodule, and possible hemorrhagic components have low SI (Fig. 7.12). On unenhanced T1-weighted images, the lesion is of variable SI depending on the contents. On postcontrast CT and MRI images, there is enhancement of the capsule as well as of internal septations and/or solid components, when present, making the internal architecture of the lesion better delineated (Figs. 7.11 and 7.12). In general, the lesions do not show restricted diffusion, except when there are thickened septations and/or mural nodularity/solid components.

The major differential diagnosis of MCN includes side-branch IPMN, oligocystic SCA, and pseudocyst. Other much more uncommon lesions are cystic lymphangioma, lymphoepithelial cysts, retention cysts, as well as cystic-degenerated PDACs or PNETs.

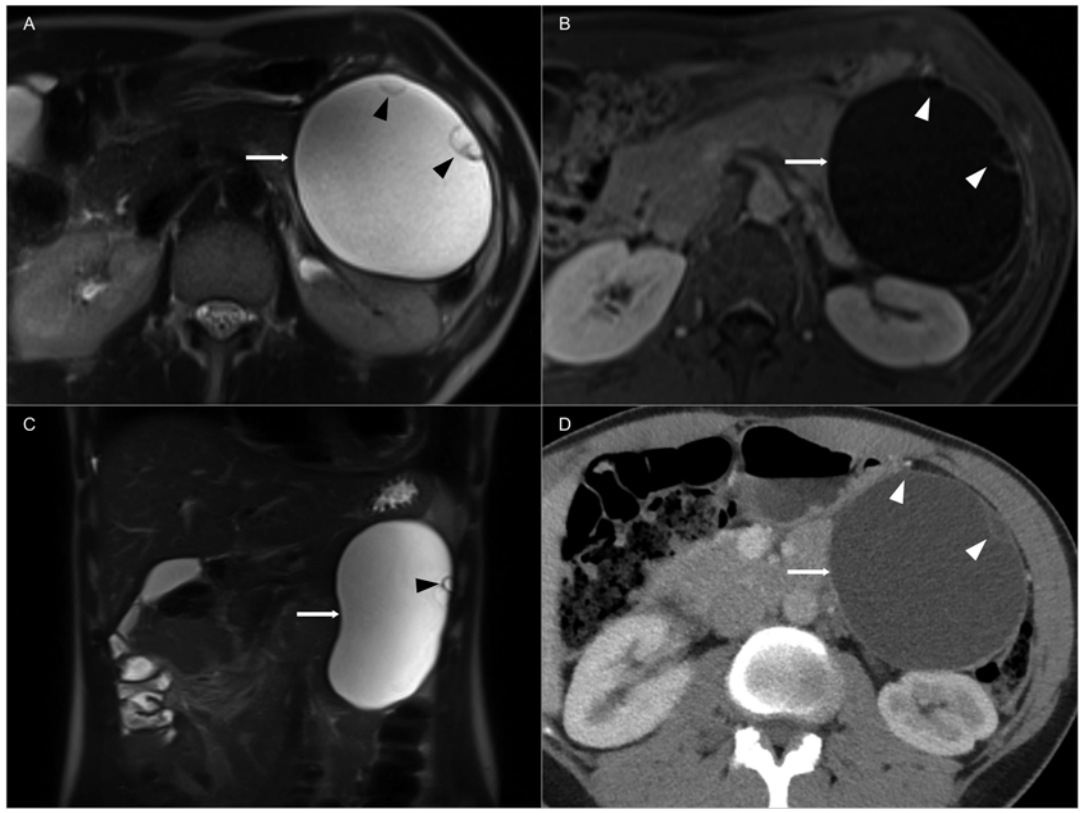

Fig. 7.12 Typical imaging findings of a female patient with a large mucinous cystic neoplasm at the pancreatic tail on MRI (**a**–**c**) and CT (**d**). The lesion (*arrow*) is unilocular with homogeneous content and two mural nodules (*arrowheads*), more easily appreciated on T2-weighted sequences [axial (**a**) and coronal (**c**) T2-weighted images]. No signs of malignancy were identified on histopathology after surgery

Intraductal Papillary Mucinous Neoplasms

These lesions are classified into the main-duct (MD) type, which can be diffuse or segmental, side-branch duct (SB) type, or mixed-type IPMN [76]. There is a varying degree of dysplasia (from mild to moderate to high dysplasia/carcinoma in situ) or even invasive carcinoma. Many authors have described various findings that increase the risk of malignancy in cases of IPMNs. Among these are the degree of MPD widening (when the diameter is 5–9 mm, it is reported to be a worrisome feature and when ≥10 mm is a high-risk finding), the existence of mural nodules/solid components, wall thickening, enhancement of the ductal wall, invasion of adjacent structures, and dilation of the CBD as well as—only in cases of SB type—progressively increasing size or size >3 cm [24, 25, 77–83]. All of the above-

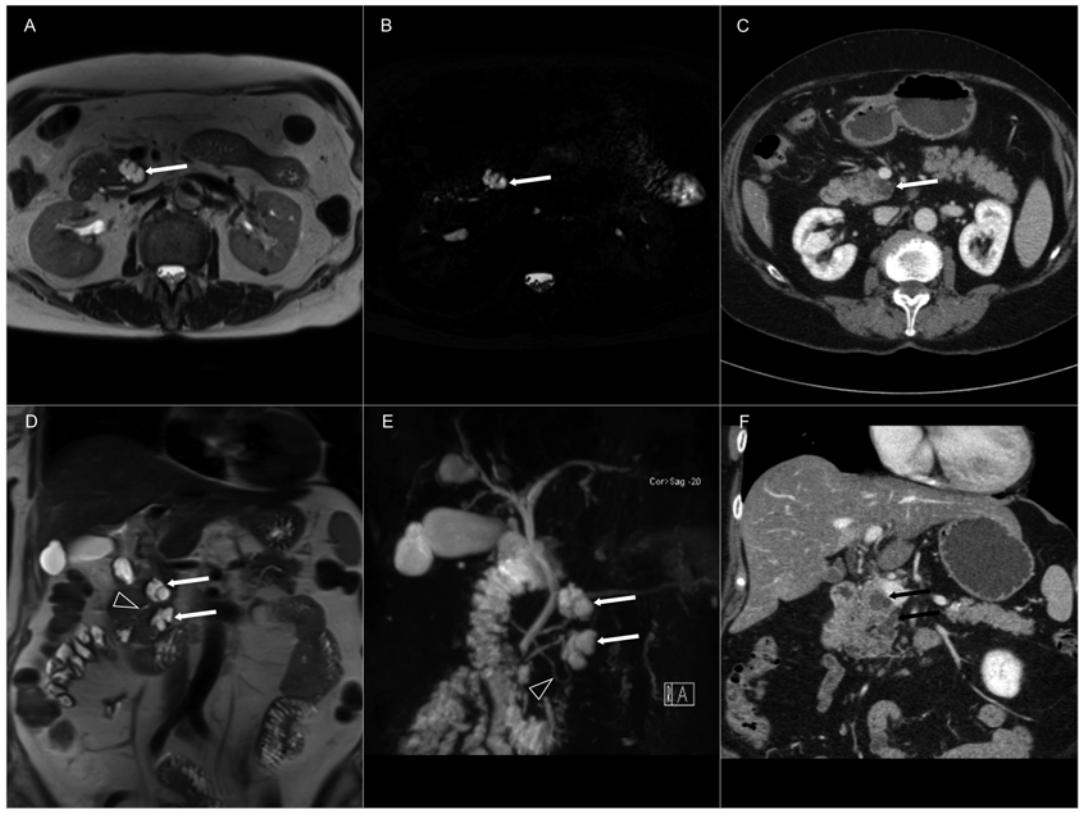

Fig. 7.13 Typical imaging findings of a patient with two side-branch IPMN lesions at the pancreatic head and uncinate process, respectively. Both lesions (*arrows*) are multilocular and lobulated, have thin internal septations, and communicate with the pancreatic ductal system (*arrowhead*), which is easier to demonstrate on the T2-weighted sequences [axial (**a**) and coronal (**d**) images) and especially on MRCP [axial thin-slice (**b**) and coronal MIP (**e**) images] compared to postcontrast CT [axial (**c**) and coronal (**f**) images]

described findings have to be carefully evaluated and taken into account, but it is advisable to avoid relying dogmatically on these predicting factors on an individual basis, as there exists no universally applicable rule [67]. SB- and mixed-type IPMNs communicate with the MPD, a key feature for their differentiation from all other cystic neoplasms.

On US, there is dilation of the MPD or a well-defined hypoechoic lesion with posterior acoustic enhancement near the MPD, in cases of MD- or SB-IPMN, respectively. The communication of the SB-IPMN with the MPD is difficult to demonstrate. On both CT and MRI, SB-IPMN is depicted as a well-defined lesion of low density (CT) or intensity (MRI) communicating or lying

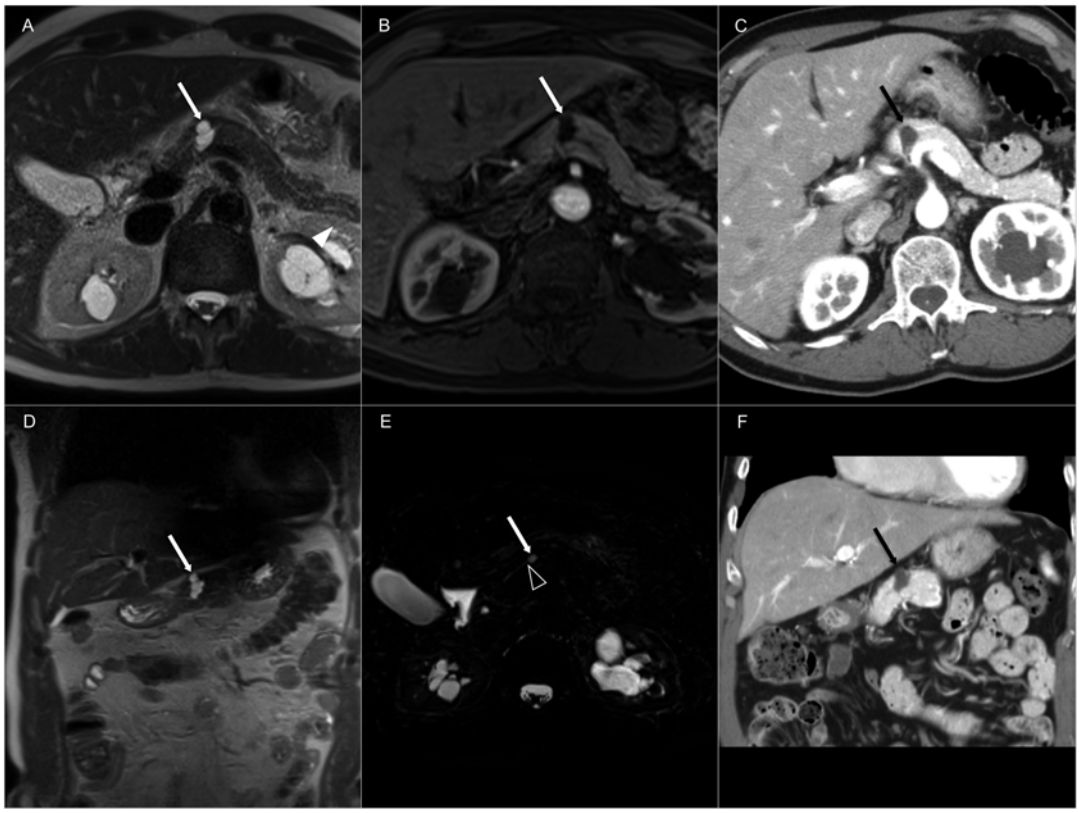

Fig. 7.14 Typical imaging findings of a patient with a side-branch IPMN at the pancreatic body on MRI (**a**, **b**, **d**, **e**) and CT (**c**, **f**). The lesion (*arrow*) has a slightly lobular contour, has a couple of thin internal septations, and shows communication with the pancreatic ductal system (*arrowhead*), nicely depicted on the thin-slice axial MRCP image (**e**). No pathological cyst wall enhancement or nodularity is seen on postcontrast images (**b**, **c**, **f**)

very near the MPD, sometimes with a typical appearance of a "cluster of grapes" (Figs. 7.13 and 7.14). MRI, and especially MRCP, is more reliable in demonstrating the communication to MPD compared to CT (Fig. 7.14e) [84]. Accordingly on both CT and MRI, MD-IPMN is depicted as a dilation of the duct, either diffusely or segmentally. Mixed-type has imaging findings of both MD- and SB-IPMN (Fig. 7.15). For all types, signs suspicious of malignancy, as described earlier in the same section, can be shown on pre- and/or postcontrast image series. The differential diagnosis of SB-IPMN includes, mainly, MCN, oligocystic SCA, and pseudocyst, while for MD-IPMN chronic pancreatitis, which may also present with diffuse or segmental dilation of the MPD [85]. For the differentiation of benign from malignant IPMNs, the DWI-based

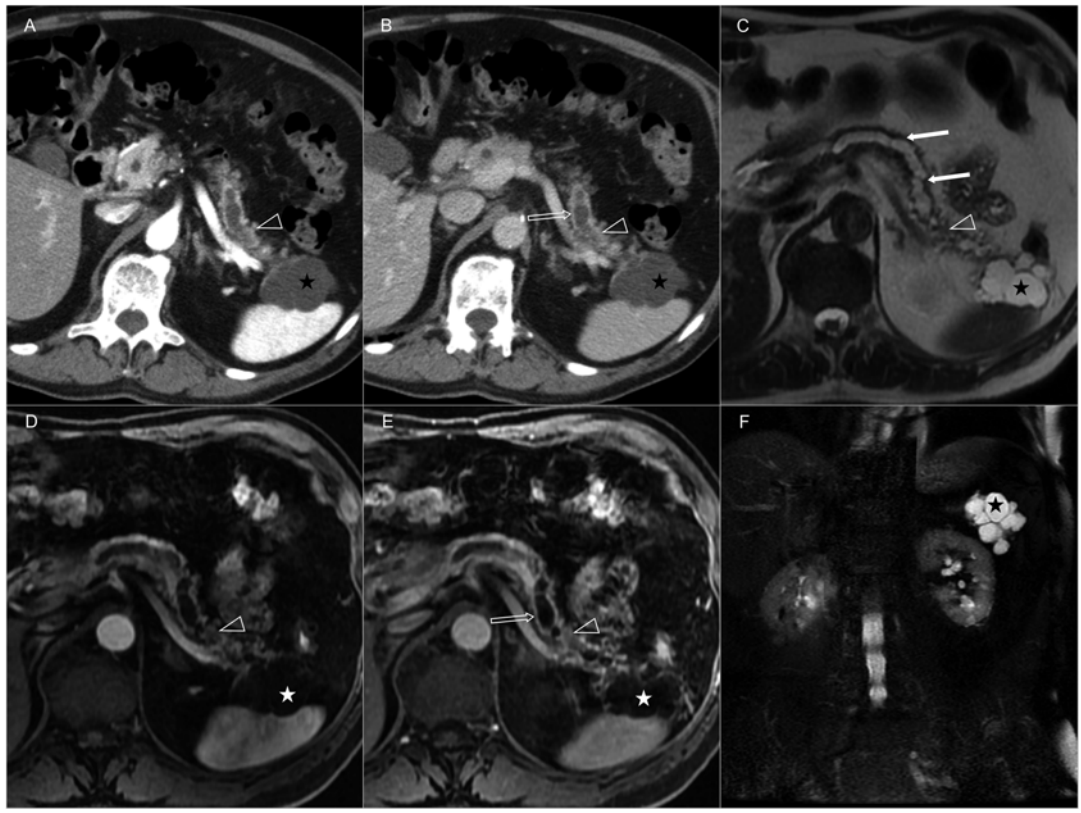

Fig. 7.15 Imaging features of a patient with mixed-type IPMN on axial CT (**a**, **b**) and MRI (**c**–**f**) images. There is a relatively smooth dilation of the main pancreatic duct (*arrow*) and a multilocular, lobulated cystic lesion (*asterisk*) at the tip of the pancreatic tail. In the tail, the wall of the main pancreatic duct shows contrast enhancement (*open arrow*) and a solid component (*arrowhead*), findings suspicious of malignancy. At histopathology after surgery, there was a varying degree of dysplasia and focal areas of invasive carcinoma

IVIM model and ^{18}F-FDG PET/CT have been reported to have promising results [43, 86].

References

1. Tempero MA, Arnoletti JP, Behrman SW, Ben-Josef E, Benson 3rd AB, Casper ES, et al. National Comprehensive Cancer Networks. Pancreatic Adenocarcinoma, version 2.2012: featured updates to the NCCN guidelines. J Natl Compr Canc Netw. 2012;10:703–13.
2. Schueller G, Schima W, Schueller-Weidekamm C, Weber M, Stift A, Gnant M, et al. Multidetector CT of pancreas: effects of contrast material flow rate and individualized scan delay on enhancement of pancreas and tumor contrast. Radiology. 2006;241:441–8.
3. Prokesch RW, Chow LC, Beaulieu CF, Nino-Murcia M, Mindelzun RE, Bammer R, et al. Local staging of pancreatic carcinoma with multi-detector row CT: use of curved planar reformations initial experience. Radiology. 2002;225:759–65.
4. Horton KM, Fishman EK. Volume-rendered 3D CT of the mesenteric vasculature: normal anatomy, anatomic variants, and pathologic conditions. Radiographics. 2002;22:161–72.
5. Horton KM. Multidetector CT, and three-dimensional imaging of the pancreas: state of the art. J Gastrointest Surg. 2002;6:126–8.
6. Horton KM, Fishman EK. Multidetector CT angiography of pancreatic carcinoma: part 2, evaluation of venous involvement. AJR Am J Roentgenol. 2002;178:833–6.
7. Horton KM, Fishman EK. Multidetector CT angiography of pancreatic carcinoma: part I, evaluation of arterial involvement. AJR Am J Roentgenol. 2002;178:827–31.
8. Kambadakone AR, Sahani DV. Body perfusion CT: technique, clinical applications, and advances. Radiol Clin North Am. 2009;47:161–78. doi:10.1016/j.rcl.2008.11.003.

9. Tirkes T, Menias CO, Sandrasegaran K. MR imaging techniques for pancreas. Radiol Clin North Am. 2012;50:379–93. doi:10.1016/j.rcl.2012.03.003.
10. Le Bihan D. Molecular diffusion, tissue microdynamics and microstructure. NMR Biomed. 1995;8: 375–86.
11. Koh DM, Collins DJ, Orton MR. Intravoxel incoherent motion in body diffusion-weighted MRI: reality and challenges. AJR Am J Roentgenol. 2011;196:1351–61. doi:10.2214/AJR.10.5515.
12. Song HK, Dougherty L. Dynamic MRI with projection reconstruction and KWIC processing for simultaneous high spatial and temporal resolution. Magn Reson Med. 2004;52:815–24.
13. Tofts PS, Brix G, Buckley DL, Evelhoch JL, Henderson E, Knopp MV, et al. Estimating kinetic parameters from dynamic contrast-enhanced T(1)-weighted MRI of a diffusable tracer: standardized quantities and symbols. J Magn Reson Imaging. 1999;10:223–32.
14. Sandrasegaran K. Functional MR, imaging of the abdomen. Radiol Clin North Am. 2014;52:883–903. doi:10.1016/j.rcl.2014.02.018.
15. Badea R, Seicean A, Diaconu B, Stan-Iuga R, Sparchez Z, Tantau M, et al. Contrast-enhanced ultrasound of the pancreas—a method beyond its potential or a new diagnostic standard? J Gastrointestin Liver Dis. 2009;18:237–42.
16. Kitano M, Kudo M, Sakamoto H, Komaki T. Endoscopic ultrasonography and contrast-enhanced endoscopic ultrasonography. Pancreatology. 2011;11 Suppl 2:28–33. doi:10.1159/000323493.
17. van Essen M, Sundin A, Krenning EP, Kwekkeboom DJ. Neuroendocrine tumours: the role of imaging for diagnosis and therapy. Nat Rev Endocrinol. 2014;10:102–14. doi:10.1038/nrendo.2013.246.
18. Rufini V, Baum RP, Castaldi P, Treglia G, De Gaetano AM, Carreras C, et al. Role of PET/CT in the functional imaging of endocrine pancreatic tumors. Abdom Imaging. 2012;37:1004–20. doi:10.1007/s00261-012-9871-9.
19. Nensa F, Beiderwellen K, Heusch P, Wetter A. Clinical applications of PET/MR: current status and future perspectives. Diagn Interv Radiol. 2014;20(5):438–47. doi:10.5152/dir.14008.
20. Schima W, Függer R, Schober E, Oettl C, Wamser P, Grabenwöger F, et al. Diagnosis and staging of pancreatic cancer: comparison of mangafodipir trisodium-enhanced MR imaging and contrast-enhanced helical hydro-CT. AJR Am J Roentgenol. 2002;179:717–24.
21. Schima W, Ba-Ssalamah A, Goetzinger P, Scharitzer M, Koelblinger C. State-of-the-art magnetic resonance imaging of pancreatic cancer. Top Magn Reson Imaging. 2007;18:421–9. doi:10.1097/rmr.0b013e31816459e0.
22. Sahani DV, Kambadakone A, Macari M, Takahashi N, Chari S, Fernandez-del Castillo C. Diagnosis and management of cystic pancreatic lesions. AJR Am J Roentgenol. 2013;200:343–54. doi:10.2214/AJR.12.8862.
23. Berland LL, Silverman SG, Gore RM, Mayo-Smith WW, Megibow AJ, Yee J, et al. Managing incidental findings on abdominal CT: white paper of the ACR Incidental Findings Committee. J Am Coll Radiol. 2010;7:754–73. doi:10.1016/j.jacr.2010.06.013.
24. Tanaka M, Fernández-del Castillo C, Adsay V, Chari S, Falconi M, Jang JY, et al. International consensus guidelines 2012 for the management of IPMN and MCN of the pancreas. Pancreatology. 2012;12:183–97. doi:10.1016/j.pan.2012.04.004.
25. Del Chiaro M, Verbeke C, Salvia R, Klöppel G, Werner J, McKay C, et al. European experts' consensus statement on cystic tumours of the pancreas. Dig Liver Dis. 2013;45:703–11. doi:10.1016/j.dld.2013.01.010.
26. Macari M, Lee T, Kim S, Jacobs S, Megibow AJ, Hajdu C, et al. Is gadolinium necessary for MRI follow-up evaluation of cystic lesions in the pancreas? Preliminary results. AJR Am J Roentgenol. 2009;192:159–64. doi:10.2214/AJR.08.1068.
27. Nougaret S, Reinhold C, Chong J, Escal L, Mercier G, Fabre JM, et al. Incidental pancreatic cysts: natural history and diagnostic accuracy of a limited serial pancreatic cyst MRI protocol. Eur Radiol. 2014;24:1020–9. doi:10.1007/s00330-014-3112-2.
28. Saif MW. Pancreatic neoplasm in 2011: an update. JOP. 2011;12:316–21.
29. Oberg K. Pancreatic endocrine tumors. Semin Oncol. 2010;37:594–618. doi:10.1053/j.seminoncol.2010.10.014.
30. Horton KM, Fishman EK. Adenocarcinoma of the pancreas: CT imaging. Radiol Clin North Am. 2002;40:1263–72.
31. Miller FH, Rini NJ, Keppke AL. MRI of adenocarcinoma of the pancreas. AJR Am J Roentgenol. 2006;187:W365–74.
32. Kim JH, Park SH, Yu ES, Kim MH, Kim J, Byun JH, et al. Visually isoattenuating pancreatic adenocarcinoma at dynamic-enhanced CT: frequency, clinical and pathologic characteristics, and diagnosis at imaging examinations. Radiology. 2010;257:87–96. doi:10.1148/radiol.10100015.
33. Prokesch RW, Schima W, Chow LC, Jeffrey RB. Multidetector CT of pancreatic adenocarcinoma: diagnostic advances and therapeutic relevance. Eur Radiol. 2003;13:2147–54.
34. Valls C, Andía E, Sanchez A, Fabregat J, Pozuelo O, Quintero JC, et al. Dual-phase helical CT of pancreatic adenocarcinoma: assessment of resectability before surgery. AJR Am J Roentgenol. 2002;178:821–6.
35. Coakley FV, Hanley-Knutson K, Mongan J, Barajas R, Bucknor M, Qayyum A. Pancreatic imaging mimics: part 1, imaging mimics of pancreatic adenocarcinoma. AJR Am J Roentgenol. 2012;199:301–8. doi:10.2214/AJR.11.7907.
36. Ichikawa T, Sou H, Araki T, Arbab AS, Yoshikawa T, Ishigame K, et al. Duct-penetrating sign at MRCP: usefulness for differentiating inflammatory pancreatic mass from pancreatic carcinomas. Radiology. 2001;221:107–16.
37. Sahani DV, Sainani NI, Deshpande V, Shaikh MS, Frinkelberg DL, Fernandez-del Castillo C. Autoimmune pancreatitis: disease evolution, stag-

ing, response assessment, and CT features that predict response to corticosteroid therapy. Radiology. 2009;250:118–29. doi:10.1148/radiol.2493080279.
38. Lu N, Feng XY, Hao SJ, Liang ZH, Jin C, Qiang JW, et al. 64-slice CT perfusion imaging of pancreatic adenocarcinoma and mass-forming chronic pancreatitis. Acad Radiol. 2011;18:81–8. doi:10.1016/j.acra.2010.07.012.
39. Kim JH, Lee JM, Park JH, Kim SC, Joo I, Han JK, et al. Solid pancreatic lesions: characterization by using timing bolus dynamic contrast-enhanced MR imaging assessment—a preliminary study. Radiology. 2013;266:185–96. doi:10.1148/radiol.12120111.
40. Fattahi R, Balci NC, Perman WH, Hsueh EC, Alkaade S, Havlioglu N, et al. Pancreatic diffusion-weighted imaging (DWI): comparison between mass-forming focal pancreatitis (FP), pancreatic cancer (PC), and normal pancreas. J Magn Reson Imaging. 2009;29:350–6. doi:10.1002/jmri.21651.
41. Lee SS, Byun JH, Park BJ, Park SH, Kim N, Park B, et al. Quantitative analysis of diffusion-weighted magnetic resonance imaging of the pancreas: usefulness in characterizing solid pancreatic masses. J Magn Reson Imaging. 2008;28:928–36. doi:10.1002/jmri.21508.
42. Klauss M, Lemke A, Grünberg K, Simon D, Re TJ, Wente MN, et al. Intravoxel incoherent motion MRI for the differentiation between mass forming chronic pancreatitis and pancreatic carcinoma. Invest Radiol. 2011;46:57–63. doi:10.1097/RLI.0b013e3181fb3bf2.
43. Kang KM, Lee JM, Yoon JH, Kiefer B, Han JK, Choi BI. Intravoxel incoherent motion diffusion-weighted MR imaging for characterization of focal pancreatic lesions. Radiology. 2014;270:444–53. doi:10.1148/radiol.13122712.
44. Imdahl A, Nitzsche E, Krautmann F, Högerle S, Boos S, Einert A, et al. Evaluation of positron emission tomography with 2-[18F]fluoro-2-deoxy-D-glucose for the differentiation of chronic pancreatitis and pancreatic cancer. Br J Surg. 1999;86:194–9.
45. Lee TY, Kim MH, do Park H, Seo DW, Lee SK, Kim JS, et al. Utility of 18F-FDG PET/CT for differentiation of autoimmune pancreatitis with atypical pancreatic imaging findings from pancreatic cancer. AJR Am J Roentgenol. 2009;193:343–8. doi:10.2214/AJR.08.2297.
46. Ozaki Y, Oguchi K, Hamano H, Arakura N, Muraki T, Kiyosawa K, et al. Differentiation of autoimmune pancreatitis from suspected pancreatic cancer by fluorine-18 fluorodeoxyglucose positron emission tomography. J Gastroenterol. 2008;43:144–51. doi:10.1007/s00535-007-2132-y.
47. Herwick S, Miller FH, Keppke AL. MRI of islet cell tumors of the pancreas. AJR Am J Roentgenol. 2006;187:W472–80.
48. Gallotti A, Johnston RP, Bonaffini PA, Ingkakul T, Deshpande V, Fernández-del Castillo C, et al. Incidental neuroendocrine tumors of the pancreas: MDCT findings and features of malignancy. AJR Am J Roentgenol. 2013;200:355–62. doi:10.2214/AJR.11.8037.
49. Poultsides GA, Huang LC, Chen Y, Visser BC, Pai RK, Jeffrey RB, et al. Pancreatic neuroendocrine tumors: radiographic calcifications correlate with grade and metastasis. Ann Surg Oncol. 2012;19:2295–303. doi:10.1245/s10434-012-2305-7.
50. Sheth S, Hruban RK, Fishman EK. Helical CT of islet cell tumors of the pancreas: typical and atypical manifestations. AJR Am J Roentgenol. 2002;179:725–30.
51. Kawamoto S, Shi C, Hruban RH, Choti MA, Schulick RD, Fishman EK, et al. Small serotonin-producing neuroendocrine tumor of the pancreas associated with pancreatic duct obstruction. AJR Am J Roentgenol. 2011;197:W482–8. doi:10.2214/AJR.10.5428.
52. Schmid-Tannwald C, Schmid-Tannwald CM, Morelli JN, Neumann R, Haug AR, Jansen N, et al. Comparison of abdominal MRI with diffusion-weighted imaging to 68Ga-DOTATATE PET/CT in detection of neuroendocrine tumors of the pancreas. Eur J Nucl Med Mol Imaging. 2013;40:897–907. doi:10.1007/s00259-013-2371-5.
53. de Herder WW, Kwekkeboom DJ, Valkema R, Feelders RA, van Aken MO, Lamberts SW, et al. Neuroendocrine tumors and somatostatin: imaging techniques. J Endocrinol Invest. 2005;28(11 Suppl International):132–6.
54. Christ E, Wild D, Forrer F, Brändle M, Sahli R, Clerici T, et al. Glucagon-like peptide-1 receptor imaging for localization of insulinomas. J Clin Endocrinol Metab. 2009;94:4398–405. doi:10.1210/jc.2009-1082.
55. d'Assignies G, Couvelard A, Bahrami S, Vullierme MP, Hammel P, Hentic O, et al. Pancreatic endocrine tumors: tumor blood flow assessed with perfusion CT reflects angiogenesis and correlates with prognostic factors. Radiology. 2009;250:407–16. doi:10.1148/radiol.2501080291.
56. Wang Y, Chen ZE, Yaghmai V, Nikolaidis P, McCarthy RJ, Merrick L, et al. Diffusion-weighted MR imaging in pancreatic endocrine tumors correlated with histopathologic characteristics. J Magn Reson Imaging. 2011;33(5):1071–9. doi:10.1002/jmri.22541.
57. Jang KM, Kim SH, Lee SJ, Choi D. The value of gadoxetic acid-enhanced and diffusion-weighted MRI for prediction of grading of pancreatic neuroendocrine tumors. Acta Radiol. 2014;55:140–8. doi:10.1177/0284185113494982.
58. Bhosale PR, Menias CO, Balachandran A, Tamm EP, Charnsangavej C, Francis IR, et al. Vascular pancreatic lesions: spectrum of imaging findings of malignant masses and mimics with pathologic correlation. Abdom Imaging. 2013;38:802–17. doi:10.1007/s00261-012-9954-7.
59. Fernández-del Castillo C, Warshaw AL. Cystic tumors of the pancreas. Surg Clin North Am. 1995;75:1001–16.
60. Sarr MG, Murr M, Smyrk TC, Yeo CJ, Fernandez-del-Castillo C, Hawes RH, et al. Primary cystic neoplasms of the pancreas. Neoplastic disorders of emerging importance—current state-of-the-art and unanswered questions. J Gastrointest Surg. 2003;7:417–28.
61. Choi JY, Kim MJ, Lee JY, Lim JS, Chung JJ, Kim KW, et al. Typical and atypical manifestations of

serous cystadenoma of the pancreas: imaging findings with pathologic correlation. AJR Am J Roentgenol. 2009;193:136–42. doi:10.2214/AJR.08.1309.
62. Barral M, Soyer P, Dohan A, Laurent V, Hoeffel C, Fishman EK, et al. Magnetic resonance imaging of cystic pancreatic lesions in adults: an update in current diagnostic features and management. Abdom Imaging. 2014;39:48–65. doi:10.1007/s00261-013-0048-y.
63. Chu LC, Singhi AD, Hruban RH, Fishman EK. Characterization of pancreatic serous cystadenoma on dual-phase multidetector computed tomography. J Comput Assist Tomogr. 2014;38:258–63. doi:10.1097/RCT.10.1097/RCT.0b013e3182ab1556.
64. Takeshita K, Kutomi K, Takada K, Kohtake H, Furui S, Takada T, et al. Unusual imaging appearances of pancreatic serous cystadenoma: correlation with surgery and pathologic analysis. Abdom Imaging. 2005;30:610–5.
65. Mottola JC, Sahni VA, Erturk SM, Swanson R, Banks PA, Mortele KJ. Diffusion-weighted MRI of focal cystic pancreatic lesions at 3.0-Tesla: preliminary results. Abdom Imaging. 2012;37:110–7. doi:10.1007/s00261-011-9737-6.
66. Khurana B, Mortelé KJ, Glickman J, Silverman SG, Ros PR. Macrocystic serous adenoma of the pancreas: radiologic-pathologic correlation. AJR Am J Roentgenol. 2003;181:119–23.
67. Dewhurst CE, Mortele KJ. Cystic tumors of the pancreas: imaging and management. Radiol Clin North Am. 2012;50:467–86. doi:10.1016/j.rcl.2012.03.001.
68. Visser BC, Yeh BM, Qayyum A, Way LW, McCulloch CE, Coakley FV. Characterization of cystic pancreatic masses: relative accuracy of CT and MRI. AJR Am J Roentgenol. 2007;189:648–56.
69. Procacci C, Carbognin G, Accordini S, Biasiutti C, Guarise A, Lombardo F, et al. CT features of malignant mucinous cystic tumors of the pancreas. Eur Radiol. 2001;11:1626–30.
70. Crippa S, Salvia R, Warshaw AL, Domínguez I, Bassi C, Falconi M, et al. Mucinous cystic neoplasm of the pancreas is not an aggressive entity: lessons from 163 resected patients. Ann Surg. 2008;247:571–9. doi:10.1097/SLA.0b013e31811f4449.
71. Goh BK, Tan YM, Chung YF, Chow PK, Cheow PC, Wong WK, et al. A review of mucinous cystic neoplasms of the pancreas defined by ovarian-type stroma: clinicopathological features of 344 patients. World J Surg. 2006;30:2236–45.
72. Nadig SN, Pedrosa I, Goldsmith JD, Callery MP, Vollmer CM. Clinical implications of mucinous nonneoplastic cysts of the pancreas. Pancreas. 2012;41:441–6. doi:10.1097/MPA.0b013e318229b9b8.
73. Sarr MG, Kendrick ML, Nagorney DM, Thompson GB, Farley DR, Farnell MB. Cystic neoplasms of the pancreas: benign to malignant epithelial neoplasms. Surg Clin North Am. 2001;81:497–509.
74. Balci NC, Semelka RC. Radiologic features of cystic, endocrine and other pancreatic neoplasms. Eur J Radiol. 2001;38:113–9.
75. Chalian H, Töre HG, Miller FH, Yaghmai V. CT attenuation of unilocular pancreatic cystic lesions to differentiate pseudocysts from mucin-containing cysts. JOP. 2011;12:384–8.
76. Procacci C, Megibow AJ, Carbognin G, Guarise A, Spoto E, Biasiutti C, et al. Intraductal papillary mucinous tumor of the pancreas: a pictorial essay. Radiographics. 1999;19:1447–63.
77. Pedrosa I, Boparai D. Imaging considerations in intraductal papillary mucinous neoplasms of the pancreas. World J Gastrointest Surg. 2010;2:324–30. doi:10.4240/wjgs.v2.i10.324.
78. Arakawa A, Yamashita Y, Namimoto T, Tang Y, Tsuruta J, Kanemitsu K, et al. Intraductal papillary tumors of the pancreas. Histopathologic correlation of MR cholangiopancreatography findings. Acta Radiol. 2000;41:343–7.
79. Irie H, Honda H, Aibe H, Kuroiwa T, Yoshimitsu K, Shinozaki K, et al. MR cholangiopancreatographic differentiation of benign and malignant intraductal mucin-producing tumors of the pancreas. AJR Am J Roentgenol. 2000;174:1403–8.
80. Choi BS, Kim TK, Kim AY, Kim KW, Park SW, Kim PN, et al. Differential diagnosis of benign and malignant intraductal papillary mucinous tumors of the pancreas: MR cholangiopancreatography and MR angiography. Korean J Radiol. 2003;4:157–62.
81. Maire F, Voitot H, Aubert A, Palazzo L, O'Toole D, Couvelard A, et al. Intraductal papillary mucinous neoplasms of the pancreas: performance of pancreatic fluid analysis for positive diagnosis and the prediction of malignancy. Am J Gastroenterol. 2008;103:2871–7. doi:10.1111/j.1572-0241.2008.02114.x.
82. Werner JB, Bartosch-Härlid A, Andersson R. Cystic pancreatic lesions: current evidence for diagnosis and treatment. Scand J Gastroenterol. 2011;46:773–88. doi:10.3109/00365521.2011.551892.
83. Manfredi R, Graziani R, Motton M, Mantovani W, Baltieri S, Tognolini A, et al. Main pancreatic duct intraductal papillary mucinous neoplasms: accuracy of MR imaging in differentiation between benign and malignant tumors compared with histopathologic analysis. Radiology. 2009;253:106–15. doi:10.1148/radiol.2531080604.
84. Waters JA, Schmidt CM, Pinchot JW, White PB, Cummings OW, Pitt HA, et al. CT vs MRCP: optimal classification of IPMN type and extent. J Gastrointest Surg. 2008;12:101–9.
85. Akisik MF, Sandrasegaran K, Aisen AA, Maglinte DD, Sherman S, Lehman GA. Dynamic secretin-enhanced MR cholangiopancreatography. Radiographics. 2006;26:665–77.
86. Sperti C, Bissoli S, Pasquali C, Frison L, Liessi G, Chierichetti F, et al. 18-fluorodeoxyglucose positron emission tomography enhances computed tomography diagnosis of malignant intraductal papillary mucinous neoplasms of the pancreas. Ann Surg. 2007;246:932–7; discussion 937–9.